Mechanics Modeling of Tendon-Driven Continuum Manipulators

David B. Camarillo, *Member, IEEE*, Christopher F. Milne, Christopher R. Carlson, Michael R. Zinn, *Member, IEEE*, and J. Kenneth Salisbury, *Member, IEEE*

***Abstract*—Continuumrobotic manipulators articulate due to their inherent compliance. Tendon actuation leads to compression of the manipulator, extension of the actuators, and is limited by the practical constraint that tendons cannot support compression. In light of these observations, we present a new linear model for transforming desired beam configuration to tendon displacements and *vice versa*. We begin from first principles in solid mechanics by analyzing the effects of geometrically nonlinear tendon loads. These loads act both distally at the termination point and proximally along the conduit contact interface. The resulting model simplifies to a linear system including only the bending and axial modes of the manipulator as well as the actuator compliance. The model is then manipulated to form a concise mapping from beam configuration–space parameters to n redundant tendon displacements via the internal loads and strains experienced by the system. We demonstrate the utility of this model by implementing an optimal feasible controller. The controller regulates axial strain to a constant value while guaranteeing positive tendon forces and minimizing their magnitudes over a range of articulations. The mechanics-based model from this study provides insight as well as performance gains for this increasingly ubiquitous class of manipulators.**

***Index Terms*—Cable drive, elastic manipulator, flexible manipulator, kinematics, redundant tendons, robotic surgery, slack tendon, snake robot, statics, tendon drive.**

I. Introduction

ROBOTICALLY assisted surgery is becoming an accepted practice in specialties ranging from ophthalmology to interventional cardiology. Some of the benefits of robotic assistance include scaled dexterity, stable manipulation, and enhanced mobility [1]–[5]. These benefits can be leveraged for minimally invasive procedures where the surgeon's dexterity is otherwise compromised by manually operating long thin instruments. Continuum manipulators are capable of traversing tortuous anatomy through a minimally invasive approach and can be managed effectively using robotic control.

Manuscript received April 10, 2008; revised April 28, 2008. First published October 28, 2008; current version published December 30, 2008. This paper was recommended for publication by Associate Editor I.-M. Chen and Editor F. Park upon evaluation of the reviewers' comments. This work was supported in part by the Stanford Bio-X Graduate Fellowship and in part by Hansen Medical, Inc.

D. B. Camarillo and J. K. Salisbury are with the Biorobotics Laboratory, Stanford University, Stanford, CA 94305 USA (e-mail: dbcamarillo@stanford.edu; jks@robotics.stanford.edu).

C. F. Milne and C. R. Carlson are with Hansen Medical, Inc., Mountain View, CA 94043 USA (e-mail: cmilne@hansenmedical.com; ccarlson@hansenmedical.com).

M. R. Zinn is with the Department of Mechanical Engineering, University of Wisconsin, Madison, WI 53706 USA (e-mail: mzinn@wisc.edu).

Color versions of one or more of the figures in this paper available online at http://ieeexplore.ieee.org.

Digital Object Identifier 10.1109/TRO.2008.2002311

Fig. 1. Steerable cardiac catheter is a tendon-driven continuum manipulator.

In contrast to discrete or hyperredundant mechanisms with rigid links and joints, continuum manipulators are inherently compliant and articulate due to elastic deformation [6]. Their compliant nature makes continuum manipulators ideal for safe operation in constrained environments. In addition, these flexible elements lend themselves to synthesis at small scales due to their relative simplicity [7]. In this study, our continuum manipulator is a steerable catheter (see Fig. 1) that we model as a cantilever beam with embedded tendons [Fig. 2(a)].

A fundamental work on beams undergoing large dynamic deflection was by Simo and Vu-Quoc [8]. They analyzed the deflection of a flexible robot arm actuated by a torque at its base using energy methods. This paper is frequently cited as the basis for contemporary continuum robot analysis, for example, see [9]. However, millimeter scale manipulators with embedded tendons undergo significantly different loading conditions. This motivates us to take a different approach to analyzing the beam mechanics.

Tendon-driven mechanisms are largely inspired by biomechanical systems. Hirose pioneered the biomechanical study of snakes leading to an interesting and relevant manipulator named "the elastic-module tendon-driven arm" [10]. He developed a geometric model for the inverse kinematics from manipulator configuration to tendon displacement. This model assumes that the tendons are in tension at all times but does not attempt to model their stretch. Given the assumption of rigid tendons, the axial length parameter of the manipulator is also modeled as a purely geometric term in the this nonlinear kinematic model.

1552-3098/$25.00 © 2008 IEEE

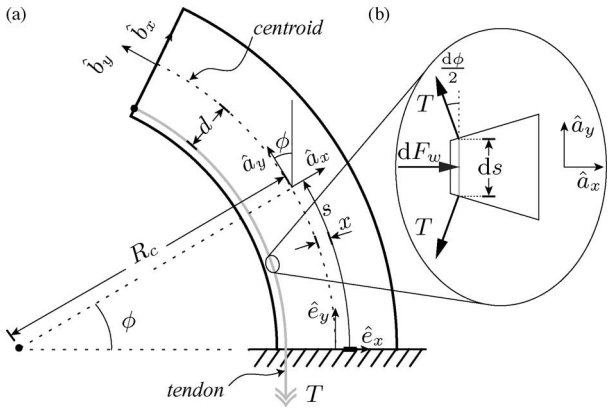

Fig. 2. Continuum manipulator diagram for a single section. (a) Cantilever beam deflected by tendon. (b) Differential tendon segment (gray).

Common to most all tendon-driven systems whether biological or not is the presence of redundant actuation. In order to maintain control of a joint in flexion and extension using tendons, one must employ antagonistic groups of tendons [11]. The Salisbury hand is an example that included four tendons to control three joints of a finger [12]. The one redundant DOF in each finger was used to tension all cables, thereby avoiding slack tendons during articulation. Preventing slack is practically important to maintain the integrity of the cable drive. Tendons in compression tend to buckle or fall off their drive pulleys resulting in actuator backlash. In a redundant system, the backlash from a slack tendon may or may not be obvious at the end effector. However, it will have a definite effect on the moment and compressive force delivered to the joint.

Although it is important to avoid tendon slack, excessive tendon loading is undesirable as well. Redundantly actuated parallel manipulators, particularly, those driven by the tendons, have been studied not only for preventing backlash (slack) but also for minimizing tendon loading [13]–[16]. Minimizing tendon load is important for medical application in which tendon size and materials are constrained by the environment. Tendon load can also have an effect on performance due to friction.

Combining tendon actuation and flexible beam dynamics, Gravagne and Walker studied the Clemson tentacle manipulator for tension-controlled vibration damping [9]. The two antagonistic tendons formed a cable loop, thereby isolating control to the bending mode (assuming no slack). Li and Rahn also studied a 1-DOF system, but with only a single tendon [17]. They carried out experiments and a mechanics analysis that included the geometric nonlinearities of tendon actuation. Given appropriate cable standoff geometry, they were able to show constant curvature deflection. This paper focused on a single-tendon-standoff at the distal termination rather than multiple proximal standoffs (or a continuous conduit in our case) which affects the mechanical interactions. In addition, the beam was assumed inextensible.

Jones and Walker developed a modular kinematic framework for a multisection elephant trunk robot [18]. One module in their framework was the tendon displacement to beam configuration mapping for a single section. This mapping was achieved by geometric kinematics and was specific to the tendon arrangement of their elephant trunk. The elephant trunk had three tendons per section which they used to model and control axial displacement. However, they did not include tendon deformation in their model. Simaan *et al.*, on the other hand, did model actuator deformation mechanics for their snake-like surgical manipulator [19]. They used an inverse kinematics model with push–pull actuators to limit loading on the primary backbone. Therefore, they did not model axial deformation of the primary backbone. In addition, their combined kinematics and mechanics operated in the inverse direction only because actuator displacement could not be used to recover its deformation and calculate manipulator configuration [20].

Our contribution is a new linear model for the forward and inverse kinematics mapping between n tendon displacements and beam configuration. The model is rooted in the mechanical interactions of the compliant tendon–beam system as a whole. This mechanics-based model is essential in achieving accurate control and avoiding slack tendons for manipulators with compliance in the axial mode and compliant tendons. This model is the first, to the best of our knowledge, that can calculate manipulator configuration explicitly from the measured displacements of n redundant tendons (assuming no slack).

To develop our model, we must closely study the internal and external effects of tendon actuation. We begin in Section II by showing that the loads from tendon actuation lead to linear elastic circular deflection and axial compression of the manipulator. Combining these mechanics with the tendon stretch and path provides the basis for our model that is presented in Section III. Accompanying the model are the conditions under which a desired configuration is feasible given the constraint that slack tendons cannot support compression. In the case of redundant tendons, we present a method for selecting an optimal solution from the set of feasible tendon forces. These considerations on slack and redundancy resolution are presented in Section IV as part of a tendon position controller that validates the complete model.

II. Single-Tendon Mechanics

Constant curvature deflection is commonly presumed for continuum manipulators in the absence of external constraints or disturbances [9], [18], [21]. For the discrete case, Higashimori *et al.* [22] analyzed the internal loading conditions (moments) from tendon actuation given a specified configuration of a gripper. For the continuous case, we examine the internal loading conditions to justify the constant curvature assumption for tendon-driven continuum manipulators undergoing large deflection in free space. The result of these mechanics also shows linear elastic deformation in bending and axial compression.

To establish the framework for the mechanics-based model, we start with a simple planar cantilevered beam undergoing large deflection. This beam is representative of a single section in a continuum manipulator. The beam is subject to multiple external axial and transverse loads as a result of actuation by a single tendon. We begin with the premise of constant curvature beam deflection and solve for the subsequent internal loads.

Given a set of material assumptions, we use these internal loads to show consistency with the assumed circular deflection. These material assumptions also lead to linear elastic bending and axial deflections from the tendon actuation. Our analytical findings are then supported with experimental evidence.

A. Internal Beam Loading From Single Tendon

Consider a cantilever beam that, by some means of external loading, has been deflected into a circular arc. We take the approach of starting with an assumed deflection solution because of the geometric nonlinearities associated with deflecting over large angles. Such a cantilever beam is pictured in Fig. 2(a) with a single tendon (gray). The beam is composed of infinite concentric arcs, one of which is shown just to the right of the centroid. Any one of these circular curves can be described by

$$\phi(s) = \left(\frac{1}{R_c + x}\right) s \tag{1}$$

where s is the arc length from the $\hat{e}_x$-axis and $\phi(s)$ is the angle between the tangent ($\hat{a}_y$) and $\hat{e}_y$, about the $\hat{e}_z$ basis vector. R_c is the radius of the centroidal arc and x is the distance from the centroid to any other arc measured along the $\hat{a}_x$-axis. Curvature is defined as

$$\kappa := \frac{\mathrm{d}\phi}{\mathrm{d}s} \tag{2}$$

and can be used to differentiate (1) yielding the curvature of a circular arc [23]

$$\kappa(x) = \frac{1}{R_c + x}\ . \tag{3}$$

The tendon has curvature $\kappa_t = \kappa(-d)$ where d is the distance from the tendon to the centroid. Here, we are approximating the tendon to run parallel to the centroidal axis.

The first step in the analysis is to isolate a differential tendon segment to solve for the transverse contact force on the beam. Before analyzing the segment, there are two key assumptions we must mention with respect to the tendon. The first is that, internally, the tendon can only resist axial tension all the way through the termination point. Externally, the tendon can only resist locally transverse loads along its length (i.e., no friction, only contact forces). These assumptions are the equivalent of saying that the tension in the tendon is constant along its length or that it is a pure tension element. Given the original premise of circular deflection geometry, we can now carry out a static equilibrium analysis on the differential tendon section.

Fig. 2(b) shows a differential segment of the deflected tendon and beam at their contact interface in the local Frenet–Serret frame a [24]. The tendon is shown to be an infinitesimally thin tension element for ease of illustration. If the differential segment of the tendon is cut at the borders of the beam segment, we can write a force balance. The forces acting on the tendon are the tension T at both ends (acting at an angle $\mathrm{d}\phi/2$ from the centroidal axis), and the transverse contact force by the conduit $\mathrm{d}F_w$. The vertical components of the end tension cancel out,

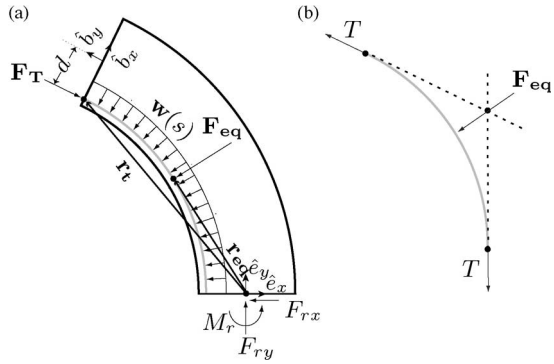

Fig. 3. Free-body diagrams. (a) Beam. (b) tendon.

and we solve for the differential transverse contact force

$$\mathrm{d}F_w = T\,\mathrm{d}\phi \tag{4}$$

that is purely in the transverse direction. If we divide (4) by $\mathrm{d}s$, we get the magnitude w of the distributed load shown in Fig. 3(a)

$$\begin{aligned} w(s) &:= \frac{\mathrm{d}F_w}{\mathrm{d}s} \\ &= T\,\kappa_t \end{aligned} \tag{5}$$

where κ_t is the constant curvature of the tendon arc. Given that this analysis holds for any arbitrary differential tendon section, we now know that the magnitude of the distributed force is constant along the length of the tendon–beam interface. Taking this result for the differential tendon segment, we can transform it back into a global beam frame and integrate to determine the cumulative effect on a transverse section of the beam.

Fig. 3(a) is a free-body diagram of the beam from the distal tip to a transversely cut section. For notational simplicity, we choose to cut at the base e frame. The external forces acting are the tendon termination force $\mathbf{F_T}$ (of magnitude T) and the distributed load $\mathbf{w}(s)$ from the tendon contact. The termination load acts longitudinally at the distal tip and the contact load acts transversely along the entire beam length. We neglect gravitational and inertial forces for a small, well-damped beam in a quasi-static configuration. The goal is to calculate the internal reaction forces (both normal and shear) and the moment on the cut surface.

We start by solving for an equivalent contact force $\mathbf{F}_{\mathrm{eq}}$ for the distributed load $\mathbf{w}(s)$. This requires integration of $\mathbf{w}(s)$ in the e frame. The Euler rotation from the base to any transverse distal section in the a frame is

$$\mathbf{R}_a^e = \begin{bmatrix} \cos\phi & -\sin\phi \\ \sin\phi & \cos\phi \end{bmatrix}. \tag{6}$$

Therefore, the distributed load can be described in the e frame by

$$\mathbf{w}(s) = \mathbf{R}_a^e\,[-T\,\kappa_t,\ 0]^T. \tag{7}$$

To get the total equivalent contact force, we must integrate over the arc length

$$\begin{aligned}\mathbf{F}_{\text{eq}} &= \int_0^{\phi_b} \mathbf{w}(s)\,\mathrm{d}s \\ &= \int_0^{\phi_b} -\kappa_t\, T\,[\cos\phi,\ \sin\phi]^T\,\frac{\mathrm{d}\phi}{\kappa_t} \\ &= T\,[-\sin\phi_b,\ \cos\phi_b - 1]^T. \end{aligned} \tag{8}$$

This force $\mathbf{F}_{\text{eq}}$ is angled directly in between the $\hat{e}_x$ and $\hat{b}_x$ basis vectors as would be expected. To find the point of application of $\mathbf{F}_{\text{eq}}$, we use a simple geometry argument. Fig. 3(b) is a free-body diagram of the tendon that must have zero total moment. The point about which the moment is most easily calculated is the intersection of the end tension forces. Since we know $\mathbf{F}_{\text{eq}}$ bisects the tension forces, it must also pass through this point. Therefore, $\mathbf{F}_{\text{eq}}$ passes through the midpoint of the arc. We use this to write the force position vectors

$$\mathbf{r_t} = [-d - 2\sin^2\phi_b)/\kappa_t,\ (2\sin\phi_b\cos\phi_b)/\kappa_t]^T \tag{9}$$

$$\mathbf{r}_{\text{eq}} = [-d - \sin^2\phi_b/\kappa_t,\ \sin\phi_b\cos\phi_b/\kappa_t]^T. \tag{10}$$

Now, all external forces and moments are defined, so we can write the static equilibrium equations and solve first for the reaction force $\mathbf{F_r}$

$$\begin{aligned}\sum \mathbf{F} &= \mathbf{0} \\ &= \mathbf{F}_{\text{eq}} + \mathbf{F_T} + \mathbf{F_r} \\ \mathbf{F_r} &= -T\,[-\sin\phi_b,\ \cos\phi_b - 1]^T - \mathbf{R}_a^e\,[0,\ -T]^T \\ &= [0,\ T]^T \end{aligned} \tag{11}$$

and then solve for the reaction moment

$$\begin{aligned}\sum M &= 0 \\ &= \mathbf{r_t} \times \mathbf{F_T} + \mathbf{r}_{\text{eq}} \times \mathbf{F}_{\text{eq}} + M_r \\ M_r &= -T\,d. \end{aligned} \tag{12}$$

The essential results of this analysis are (11) and (12). The first element of (11) says that there is no shear force experienced on the transverse section and the second says that the longitudinal normal force is exactly the tendon tension. The moment in (12) is the tendon tension multiplied by what can be viewed as a moment arm d. Note that there is no dependency on angle ϕ_b, and therefore, this result will be true for any beam articulation and for any transverse cross section along the beam's length.

B. Tendon Tension to Beam Articulation

Now that the internal loading conditions have been determined, we approach the problem from the opposite direction to show consistency with circular deflection. We then ask the question: if a cross section of material in a cantilever beam is loaded according to (11) and (12), what would be the resulting deflection? The following material assumptions are used to answer this question:

1) linear elasticity in both the axial and bending modes;
2) plain strain, meaning the material is approximately homogeneous along the longitudinal axis [25];
3) Saint Venant's principle applies for the internal load distribution being independent of the external load configuration [26];
4) planar cross sections remain planar after deflection [8];
5) material properties are symmetric about any plane containing the centroidal axis.

Since the applied moment is longitudinally invariant (12), we know that the neutral surface is symmetric about any transverse cross section given the earlier assumptions. This symmetry indicates that the beam must bend in a circular arc. By introducing the beam bend stiffness K_b, this deflection can be described as linear elastic bending

$$M = K_b\,\kappa. \tag{13}$$

To get more information about the curvature, we substitute (12) into (13) yielding the relationship between tendon tension and curvature

$$\kappa = -\left(\frac{d}{K_b}\right) T \tag{14}$$

where κ is the curvature of the neutral surface and the negative sign is due to the tendon tension being defined as a positive force. Equation (14) tells us that the beam curvature is controlled directly by the cable tension with a gain of the moment arm to bending stiffness ratio. However, the curvature we speak of is relating to the neutral surface. The next question to ask then is where does the neutral surface lie?

If we use the principle of superposition to independently consider the bending and axially compressive strains, we can solve for the location of the neutral axis. The axial (ϵ_a) and bending (ϵ_b) strains (manipulator compression defined as positive strain) for the cross section shown in Fig. 4 are

$$\epsilon_b(x) = \frac{1}{K_b}\,M_r\,x \tag{15}$$

$$= \frac{d}{K_b}\,x\,T \tag{16}$$

$$\epsilon_a = \left(\frac{1}{K_a}\right) T. \tag{17}$$

The bending strain is dependent on the distance x from the centroid along the $\hat{a}_x$-axis. The axial strain is a function of the beam tensile stiffness K_a and tension T only. When we sum these strain fields (16) and (17), the zero point defines the neutral axis as seen in Fig. 4

$$\epsilon_y(x) = \epsilon_b(x) + \epsilon_a \tag{18}$$

$$\epsilon_y(x_{na}) = 0$$

$$x_{na} = \left(\frac{K_b}{K_a}\right) d^{-1}. \tag{19}$$

The neutral axis location in (19) means that under single-tendon articulation, the neutral axis will be controlled by the design of the manipulator. The design parameters that control

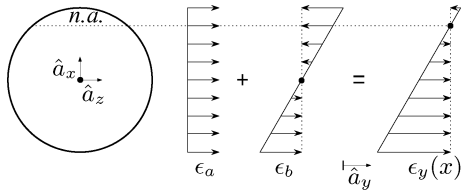

Fig. 4. Strain fields from bending and compression with resulting neutral axis. A cross section of the manipulator is shown on the left as a circle in the $\hat{a}_x$–$\hat{a}_z$ plane. The strains fields are directed in the $\hat{a}_y$ axial direction of the cross section.

the location are the tendon moment arm, and the beam bending to axial stiffness ratio. This makes intuitive sense that if a manipulator is very axially stiff with relatively small bending stiffness, the neutral axis should run almost down the centroid of the beam. The Clemson Elephant trunk [21] might be a good example of this as it is built with u-joints (high axial stiffness) and springs (lower bending stiffness).

This completes the relationship between beam articulation and the force from a single tendon. The tension will control the bend radius linearly, and the neutral axis will be statically offset from the centroid (distance dependent only on the manipulator design).

C. Mechanics Experimental Results

Here, we present experimental data to substantiate our analytical predictions and estimate the model parameters. Articulation experiments are performed on a 3.8-mm-diameter catheter (Fig. 1). The catheter is a hollow composite cylinder with a superelastic NiTi spine. The inner and outer diameters of the catheter are lined with laminated plastics for medical use. The material properties of this catheter are consistent with the aforementioned material assumptions of our model. The catheter is controlled by four equally spaced tendons that lie approximately on its perimeter within Teflon conduits. For these planar experiments, however, only a single tendon is articulated and the others are left to float freely.

The independent variables that we set are the articulating length of the manipulator and its deflection angle. The angle is set by deflecting the manipulator tip to align with the square grid in Fig. 6(a). The articulating length is set by inserting the catheter out of the support sheath before articulation. All deflections are produced by tethering a single tendon proximally to a Chatillon force gage on a linear stage. The tendon actuation is achieved by manually displacing the force gage in Fig. 5(a) and the articulation measurements are taken by eyesight with the setup in Fig. 6(a).

For a given articulating length and angle, we record measurements of the bend radius, axial compression, and tendon tension. The bend radius is measured by selecting the closest inscribed arc to a point along the manipulator's centroid. The point of choice on the centroid is that which is the greatest Euclidean distance from the manipulator origin, as seen in Fig. 6(a). The arcs are spaced at 1.25-mm resolution with respect to the radius.

Axial compression is needed to compute the net arc length and the axial strain. Axial compression is measured by the protruding length of the concentric, free-floating element routed down the catheter's working channel that is fixed proximally. Our intention is for the measurement element to remain undeformed axially as it bends with the manipulator such that its protrusion is equal to the axial deformation of the catheter. The estimated compression measurement error is ± 0.5 mm over the 770 mm catheter length. It is worth noting that the axial strains and stiffness calculated here are for the entire length of the catheter, not just the articulating beam as we have used it so far. This is because we are telescoping the catheter out of a sheath to set various articulating lengths and we do not have a method for distinguishing between proximal and distal compression. This sheath will also lead to a slight error due to the unmodeled retraction of the catheter inside the sheath from proximal compression.

Experimental data points are acquired with the manipulator articulated to $\phi = 90\,^\circ$, $180\,^\circ$, and $270\,^\circ$ at three different articulating lengths (60, 70, and 80 mm undeformed length). The most basic result is that of circular deflection. Notice that

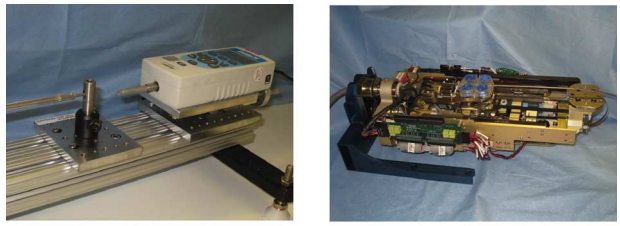

(a) (b)

Fig. 5. Two-tendon actuation mechanisms. (a) Single tendon is tethered to force gage displaced manually along the linear stage for mechanics experiments. (b) Four tendons are on pulleys and a robot is used for tendon position control experiments. The Robot has dc motors with 116:1 gear reduction and 1 000 count/rev encoders.

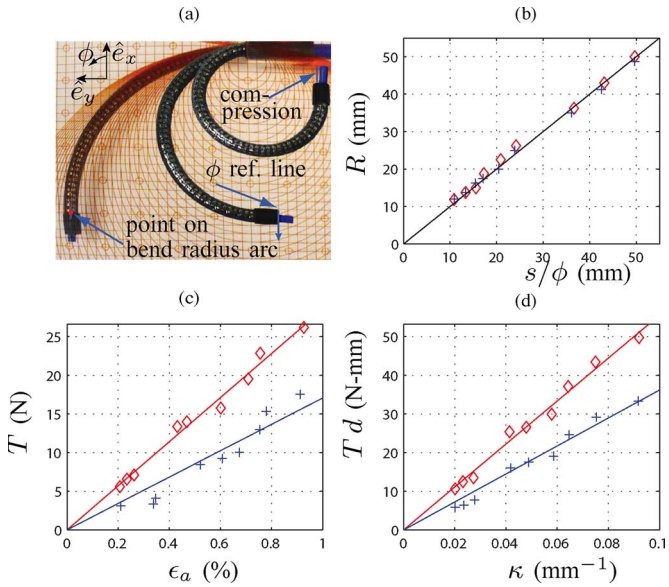

Fig. 6. Single-tendon data points reached by flexing (diamonds) and extending (crosses). (a) Experimental setup. (b) Bend curve measurements in comparison to constant curvature (solid line). (c) axial linearity with resulting average stiffness of $\bar{K}_a = 2\,281$ N. (d) Bending linearity with resulting average stiffness of $\bar{K}_b = 458$ N$\cdot$ mm^2.

the manipulator's curve approximately follows the inscribed circular arcs. To quantify the circular deflection, Fig. 6(b) plots the bend radius (R) versus the arc length to deflection angle ratio (s/ϕ). The arc length is computed as the initial undeformed length less the compression. From (1), we know this should be a line with a slope of 1, as it very nearly is.

We now examine the bending and compression data to validate (14) and (17) and estimate their stiffness parameters. Fig. 6(c) plots the axial mode's force–strain relationship and two best fit lines. There are two lines because each experiment was carried out twice, once approaching the set point in flexion and the other approaching from extension. This hysteresis is likely due to the viscoelasticity of the plastics and other frictional effects. Therefore, the average of these two slopes subtracts out the effect of friction and estimates the true stiffness value K_a from (17). Lastly, Fig. 6(d) plots the moment–curvature relationship where curvature of the neutral axis is approximated using the recorded bend radii. It demonstrates that curvature is indeed linearly related to tendon tension by K_b, thereby validating (14).

It should be noted that the observed hysteresis in Fig. 6(c) and (d) is not described by our model. We have avoided doing so to minimize model complexity, and the forthcoming control results demonstrate satisfactory performance. In addition, a teleoperated surgical system is well suited to correct for a variety or minor errors. The teleoperator will have the ability to intentionally dither out the friction if the shape of the catheter is not well matched to a constant curvature arc. For stochastic motions, friction will be zero on average serving as a natural dither for many tasks.

D. Comparison to Alternative Beam Analysis

In contrast to our approach in solving the tendon-driven continuum beam mechanics, one might resort to either a pure bending or eccentric axial loading analysis. For manipulators with very high axial to bending stiffness ratios, pure bending analysis can suffice for relatively small deflections ($<10^\circ$). However, the traditional deflection result found in tables is obtained by integration at small angles yields a quadratic form [26]. This clearly becomes erroneous for large deflections since we know the curve is circular.

Eccentric axial loading analysis for small deflections will, in fact, produce the same results at which we have arrived here. This is because the transverse tendon contact force is negligible at small angles and the tendon termination load is still geometrically linear. However, if one considers eccentric axial loading at large deflections, the tendon termination force is a follower load, and therefore, contributes a nonlinear shear component. At large deflections, it happens to be the tendon contact load itself that nullifies these would-be geometric nonlinearities. This is easiest to conceptualize if one pictures a continuum manipulator articulated at 90°. Without the tendon contact force, the base of the manipulator would be in pure shear. One can begin to see here that the existence of the tendon contact load cancels this shear and provides a compressive force that is equal to the tendon tension. Due to its overhang, the contact force also gives rise to the moment that creates the observed circular deflection.

Another aspect of our analysis that differs from other approaches is the way in which we describe the manipulator stiffnesses. Where one might be accustomed to using the quantities EI and EA in beam analysis, we instead use K_b and K_a for the beam bending and axial stiffnesses [25]. Whereas in the mechanical design process, the internal material properties and geometry are important information; in the present study, we are more interested in bulk composite manipulator properties for control. Therefore, we can operate at a higher level of abstraction and be ignorant to the internal material properties and geometry other than those pertaining to the four assumptions mentioned earlier.

Likewise, we use material strain ϵ instead of stress σ to minimize the required knowledge of internal structure parameters. This black box approach is particularly useful since materials used for continuum manipulator flexures are often composites with potentially complicated geometry. This can mean that their modes and numerical characteristics may not be well defined. Therefore, the bulk material properties should be experimentally identified.

III. Redundant Tendon Model

We extend our model to include multiple tendons that expands the range of achievable beam configurations. For the single-tendon model and experimental data, the tendon, axial, and bending modes act as serial force transmission elements. In the following extension, we assume multiple tendons to act in parallel with one another following the manipulator elements. This allows us to draw an analogy to a linear spring system for which we present the mapping from beam configuration space to the displacement of n potentially redundant tendons. We present three equivalent but complimentary forms of this redundant tendon model. The first is a mechanical schematic, the second a matrix equation, and the last an algebraic block diagram.

A. Tendon Displacements to Beam Configuration

To complete the fundamental set of equations for our mechanics model, we introduce a simple linear–elastic tendon model

$$\epsilon_t = \left(\frac{1}{K_t}\right) T, \qquad T \geq 0. \tag{20}$$

The inequality constraint implies that the tendon can only experience tension. By considering (20) simultaneously with (14) and (17), we notice that these are three linear elasticity equations all with the same force but different displacements. This motivates us to draw the analogy to a set of series springs illustrated in Fig. 7 by the solid line path. This spring model of the manipulator is composed of a rotational spring for the beam bending mode and linear displacement springs for both the tendon and the beam's axial mode. This model is very helpful in conceptualizing the transformation from desired beam articulation to forces and back to tendon displacements. Keep in mind that the tendon displacement Δl_t is not only due to its strain but also due to its motion from the ground. Therefore, the total tendon displacement must include the beam bending and axial

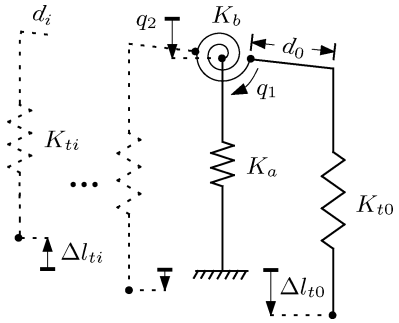

Fig. 7. Spring model for tendon-manipulator system. Shown with a single tendon (solid on right), but can be used to model n tendons (dashed on left).

compression displacements

$$\Delta l_t = l_b\,\epsilon_b(d) + l_a\,\epsilon_a + l_t\,\epsilon_t. \tag{21}$$

where l_t and l_b are the undeformed lengths of the tendon and articulating beam, respectively. l_a is the undeformed axial length and should generally be equal to l_b but, in the present study, our measurements lump the distal articulating length with the proximal length. The beam bending strain $\epsilon_b(d)$ is dependent on the distance from the centroid. By combining (13) and (15), we can express the beam bending strain along the tendon arc as

$$\epsilon_b(d) = \kappa\, d. \tag{22}$$

Before completing the mapping from beam articulation to tendon displacement, we should consider the limitation arising from the inequality of (20). If our control goal is to enforce a desired beam curvature κ, only a half-space is reachable since the tendon can only act in tension (you cannot push a rope). To span the entire space of curvature with tendon actuators, we must at least add a second tendon on the other side of the centroid. In general, when attempting to independently control m joints with n tension elements (by exerting positive or negative actuation forces), we require at least

$$n \geq m + 1 \tag{23}$$

tendons as stated in [11]. The dotted lines in Fig. 7 illustrate n tendons that could act on either side of the centroid. Note that as we add tendons, so long as the only difference is the moment arm d_i, the manipulator will obey all previous equations due to superposition.

The motivation for adding tendons was to span the entire bending space. However, when bending in one particular direction, we will have extra DOFs if multiple tendons are in tension. This allows us to introduce additional control goals. For example, in Fig. 4, we could now independently control the compression and bending strain fields ϵ_a and $\epsilon_b(x)$. We choose to express a new constraint by specifying the strain along the centroidal axis. Recall that for a single tendon, the neutral axis stayed at a fixed location offset from the centroid as described in (19). This implies that the material along the centroidal axis would deform as a function of curvature. We may reformulate (18) for multiple tendons at the centroid defined by $x = 0$

$$\begin{aligned}\epsilon_y(0) &= \epsilon_a \\ &= \frac{1}{K_a}\left(T_0 + T_1 + \cdots + T_n\right).\end{aligned} \tag{24}$$

By specifying $\epsilon_y(0)$, x_{na} will no longer be fixed, instead it will move as necessary to satisfy (24) and the bending requirement.

From here on, we assume that we have available to us n appropriately distributed tendons satisfying (23). This allows us to write the beam configuration–space description for a manipulator section with a set initial length as the vector

$$\mathbf{q} = [\kappa,\ \epsilon_a]^T. \tag{25}$$

This configuration–space description of beam strains captures the deformed loading state of the manipulator as well as its kinematic shape. With this description of configuration, we can form the relationship to tendon tension according to the spring model from (14) and (17)

$$\begin{bmatrix} K_b & 0 \\ 0 & K_a \end{bmatrix} \begin{bmatrix} \kappa \\ \epsilon_a \end{bmatrix} = \begin{bmatrix} -d_0 & -d_1 & \cdots & -d_n \\ 1 & 1 & \cdots & 1 \end{bmatrix} \begin{bmatrix} T_0 \\ T_1 \\ \vdots \\ T_n \end{bmatrix} \tag{26}$$

or in compact matrix form, the constitutive equation is

$$\mathbf{K}_m\,\mathbf{q} = \mathbf{D}\,\boldsymbol{\tau}. \tag{27}$$

where $\mathbf{K}_m$ is the stiffness matrix for the manipulator, $\mathbf{D}$ represents the tendon moment arms as well as the axially directed loads, and $\boldsymbol{\tau}$ is the tendon tension vector.

The constitutive equation (27) describes the mechanical response of the manipulator. In order to translate this response into tendon displacements, we must link the tendon tension to the tendon displacement. This can be achieved by reintroducing the tendon displacement equation (21) vectorially and combining it with the tendon elasticity (20)

$$\begin{aligned}\mathbf{y} &= [\Delta l_{t0}, \Delta l_{t1}, \ldots, \Delta l_{tn}]^T \\ &= l_b\,\kappa \begin{bmatrix} d_0 \\ d_1 \\ \vdots \\ d_n \end{bmatrix} + l_a\,\epsilon_a \begin{bmatrix} 1 \\ 1 \\ \vdots \\ 1 \end{bmatrix} + l_t\,\frac{1}{K_t} \begin{bmatrix} T_0 \\ T_1 \\ \vdots \\ T_n \end{bmatrix} \\ &= \mathbf{D}^T\,\mathbf{L}_0\,\mathbf{q} + \mathbf{L}_t\,\mathbf{K}_t^{-1}\,\boldsymbol{\tau}.\end{aligned} \tag{28}$$

We refer to (28) as conservation of strain where $\mathbf{L}_0 = \mathrm{diag}(l_b, l_a)$, $\mathbf{L}_t = \mathrm{diag}(l_t)$, and $\mathbf{K}_t^{-1} = \mathrm{diag}(1/K_t)$ assuming identical tendons. The forward and inverse kinematics model can now be solved for by combining the conservation of strain (28) and the constitutive equation (27) as

$$\mathbf{y} = \mathbf{C}_m\,\boldsymbol{\tau} \tag{29}$$

where the compliance matrix is

$$\mathbf{C}_m = \mathbf{D}^T\,\mathbf{L}_0\,\mathbf{K}_m^{-1}\,\mathbf{D} + \mathbf{L}_t\,\mathbf{K}_t^{-1}$$

leading to

$$\mathbf{y} = \mathbf{A}^{\dagger}\,\mathbf{q} \tag{30}$$

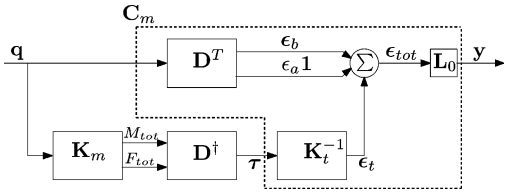

Fig. 8. Block diagram for information flow of inverse kinematics model (30).

where the forward kinematics transformation matrix is

$$\mathbf{A} = \mathbf{K}_m^{-1}\,\mathbf{D}\,\mathbf{C}_m^{-1}.$$

Equation (29) describes the input–output relationship from tendon tension to displacement. $\mathbf{C}_m$ is the square and invertible since any set of tendon displacements always has an associated set of tensions (ignoring slack for now). $\mathbf{K}_m$ is invertible as well since it is diagonal. Therefore, in (30), the generalized inverse of the forward kinematics matrix $\mathbf{A}$ boils down finding an inverse for $\mathbf{D}$ to resolve the tendon tensions. For the planar case, $\mathbf{D}$ will be invertible so long as there are at least two tendons in the set

$$\{d_i, d_j \mid d_i \neq d_j\}. \tag{31}$$

For a feasible solution to exist via tendon actuation, we must also require that

$$\boldsymbol{\tau} \geq \mathbf{0}. \tag{32}$$

Given these conditions (31) and (32), the inverse kinematics works by taking the input configuration strain $\mathbf{q}$, multiplying by $\mathbf{K}_m$ to calculate the required beam loads, then $\mathbf{D}^\dagger$ to choose consistent tendon tensions, and finally, $\mathbf{C}_m^{-1}$ to give tendon displacements $\mathbf{y}$.

B. Model Topology

In essence, (30) is a mathematical expression for the solution to the mechanical schematic illustrated in Fig. 7. When posed in a block diagram form (see Fig. 8), we can glean a physical interpretation for the information flow through the various transformations. We may also partition the block diagram to distinguish the vector spaces and the nature of the transformations.

The input to the inverse kinematics is the desired beam configuration and the output is the associated tendon displacement. The tendons must displace to account for the strains from beam bending ($\boldsymbol{\epsilon}_b$), axial compression (ϵ_a), as well as tendon stretch ($\boldsymbol{\epsilon}_t$). On the top side of the diagram, the $\mathbf{D}^T$ block performs the kinematic transformation to bending and axial strain of the beam along the tendon arcs. On the bottom half of the diagram are the mechanics transformations leading to the tendon strain. First, the beam configuration is mapped to the required beam loads $M_{\rm tot} = \sum T_i d_i$ and $F_{\rm tot} = \sum T_i$ by the stiffness block $\mathbf{K}_m$. Next, $\mathbf{D}^\dagger$ resolves any actuation redundancy and specifies how the tendon tensions $\boldsymbol{\tau}$ will be distributed and account for the desired beam loads. The tendon stiffness $\mathbf{K}_t$ is then used in the inverse sense to convert tendon tension to tendon strain $\boldsymbol{\epsilon}_t$. Once all of the strains are summed, they are multiplied by the undeformed lengths $\mathbf{L}_0$ to form the total tendon displacement $\mathbf{y}$ as the model output.

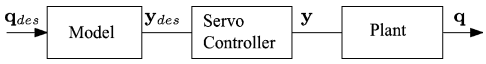

Fig. 9. Tendon position controller block diagram where "model" block contains the input filter (35) followed by the inverse kinematics from (30).

This block diagram can also operate in the reverse direction for the forward kinematics. For the forward kinematics, there will always be a solution regardless of the tendon arrangement. Imagine arbitrarily displacing the tendons in Fig. 7, a configuration will always be reached, yet not necessarily with a positive tendon tension. In reality, a negative tension would indicate that a tendon has gone slack and the output configuration is incorrect. A solution to the inverse kinematics will exist if $\mathbf{D}$ is invertible. However, there may or may not exist a solution with all positive tensions. It is the role of the control strategy to determine which $\mathbf{D}^\dagger$ to choose and protect against slack tendons in achieving a desired configuration.

IV. Tendon Position Controller

To leverage the present model relating beam configuration to tendon displacements, we implement a tendon position controller that tracks the model output. The goal is to issue a beam configuration command for a single isolated section of a continuum manipulator and for the controller to execute that command in real time. Here, we describe our control architecture including limitations we impose on inputs to allow the feasibility of a positive tendon tension. Next, we present two possible approaches to resolving any tendon redundancy and their implications on manipulator performance. We conclude by presenting data from real-time control experiments driving a catheter.

A. Control Architecture

The essence of a tendon position controller can be described by the three blocks in Fig. 9. The model block is essentially (30) with some front-end filtering to restrict allowable inputs. The servo controller block is achieved with the robot in Fig. 5(b) driving tendons on pulleys. This robot is composed of high-bandwidth current amplifiers driving dc motors with encoder feedback to close the servo loop. We assume unity gain for the servo block due to the high torque output of the robot and because the configuration input dynamics will be much slower than that of the servos or the beam dynamics. The plant is nominally the inverse of the estimated model and, barring any significant disturbances, should approximate the desired result.

The input form from (25) can be used to specify an arbitrary duple of desired curvature and axial strain $\mathbf{q}_{\rm des}$. In reality, a physical-tendon-driven manipulator cannot span this entire 2-D space. Therefore, some inputs are not attainable and should be filtered out. This can be accomplished as the first subblock within the modeling block. In designing this filter, we use the assumption that achieving the desired curvature ($\kappa_{\rm des}$) is the primary goal and that the desired axial strain ($\epsilon_{\rm des}$) is the secondary and subject to necessary modification. Of course, we can use the information from this filter to restrict the input set *a priori* so that the exact input is always achievable.

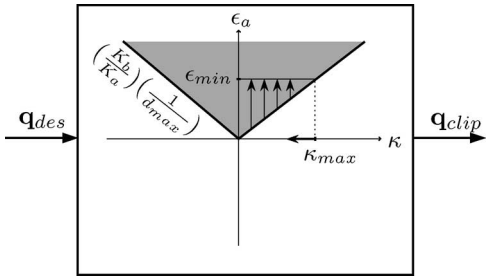

Fig. 10. Input filter to guarantee existence of a feasible solution within gray space. It also illustrates a strategy for maintaining constant axial compression by knowing the maximum desired curvature and establishing the minimum constant axial strain value.

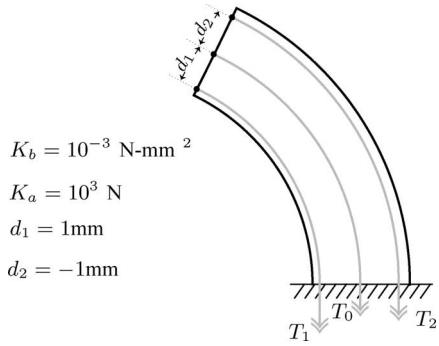

Fig. 11. Simulated three-tendon manipulator.

For bending, if (23) is satisfied, the manipulator can arbitrarily articulate about its m axes in the absence of singularities. For axial strain, however, a positive tendon tension mandates that only positive compression is possible along the centroid (24). This suggests that for a specified curvature, there exists a minimum axial compression $\epsilon_{\min}$. The minimum compression corresponds to the minimum total force. This occurs when the single outer most flexor tendon bears all of the tension because it has the largest moment arm. Using $\mathbf{D} = [d_{\max},\ 1]^T$ and the corresponding $\boldsymbol{\tau}$ in (27) allows us to solve for the minimum possible compression

$$\epsilon_{\min}(\kappa) = \left(\frac{K_b}{K_a}\right)\left(\frac{1}{d_{\max}}\right)\kappa. \tag{33}$$

With this result, we can begin to construct the input filter subblock illustrated in Fig. 10. If the desired input lies anywhere in the gray subspace, it may pass through unfiltered provided that there exists at least one pair of antagonistic tendons to generate any compression desired above the minimum. This provision can be expressed by the set $\mathbb{D}$ of a tendon pair

$$\mathbb{D} := \big\{\{d_i, d_j\} \mid (d_i \geq 0)\ \wedge\ (d_j\ \leq 0)\big\}. \tag{34}$$

If, on the other hand, all tendons are strictly on one side of the centroid or the input axial strain is less than the minimum, we must clip the axial strain to the minimum. To be complete, we must also check that the direction of the bend is possible such that at least one tendon exists on the flexion side of the bend. These rules for the filter are summarized as

$$\kappa_{\text{clip}} = \begin{cases} \kappa_{\text{des}}, \text{if } \operatorname{sgn}(\kappa_{\text{des}}) \neq \operatorname{sgn}(d_i) \\ 0, \quad \text{if } \operatorname{sgn}(\kappa_{\text{des}}) = \operatorname{sgn}(d_i) \end{cases}$$

$$\epsilon_{\text{clip}} = \begin{cases} \epsilon_{\text{des}}, & \text{if } \epsilon_{\text{des}} \geq \epsilon_{\min} \text{ and } \{d_j, d_k\} \in \mathbb{D} \\ \epsilon_{\min}(\kappa_{\text{clip}}), & \text{if } \epsilon_{\text{des}} < \epsilon_{\min} \text{ or } \{d_j, d_k\} \notin \mathbb{D} \end{cases} \tag{35}$$

where the output of the filter block is $\mathbf{q}_{\text{clip}} = [\kappa_{\text{clip}},\ \epsilon_{\text{clip}}]^T$.

Similar to the neutral axis location, the input filter of Fig. 10 is dependent on the manipulator design. Again, the bending to axial stiffness ratio shows up, now in the filter slope. If a manipulator is designed to have relatively high axial stiffness, for example, the slope will be very small and most inputs will be admissible. This makes sense because such a manipulator can bend with negligible compression but antagonistic actuation could be used to hold the bend and arbitrarily set any positive compression. Minimal filtering would then be required other than ensuring positive axial compression and potentially antagonistic actuation.

The remaining step required to implement the controller in Fig. 9 is to chose a method for computing $\mathbf{D}^\dagger$ in (30). The input filter in Fig. 10 and specified by (35) ensures that a feasible solution to (27) does exist (i.e., there is some $\boldsymbol{\tau}$ consistent with $\mathbf{q}_{\text{clip}}$ where $\boldsymbol{\tau} \geq 0$). However, a general inverse of $\mathbf{D}$ does not necessarily lead to one of these feasible solutions if it does not explicitly consider the inequality constraint on $\boldsymbol{\tau}$. In addition, there can be infinite choices for how to invert $\mathbf{D}$ that may distribute the tendon forces more or less favorably. In the following two sections, we present a minimum-norm and minimax approach to solving for $\mathbf{D}^\dagger$ in the context of these issues.

B. Minimum-Norm Solution

To study the behavior of our control solutions, we will assume that the high-level goal is to articulate a single section in bending without concerning ourselves with the axial mode. An approach to doing this is to supply a control input that keeps the axial compression constant. In choosing the specific value, we can use the knowledge of our input filter (35) to ensure that $\mathbf{q}_{\text{clip}} = \mathbf{q}_{\text{des}}$ and to allow the opportunity for $\boldsymbol{\tau} \geq \mathbf{0}$. We accomplish this while not stressing the manipulator more than necessary by choosing the constant strain

$$\epsilon_{\text{des}} = \epsilon_{\min}(\kappa_{\max}) \tag{36}$$

where $\kappa_{\max}$ is the maximum desired curvature for the specific application. This input choice is illustrated in Fig. 10 where all inputs below $\kappa_{\max}$ can be pushed up to $\epsilon_{\min}(\kappa_{\max})$ but we never exceed this minimum value.

Now that the control input is confined to a 1-D space, we construct a mathematical manipulator and simulate a simple articulation. The subject of this simulation is pictured in Fig. 11 including its numerical values. This manipulator is representative in scale of a surgical instrument. The antagonistic pair of tendons are spread as far as possible from the centroid to bring down the minimum axial strain in (33). A third tendon is positioned along the centroid providing the redundancy used for lowering tendon forces.

Our first simulation uses the minimum-norm solution, $\mathbf{D}^\dagger = \mathbf{D}^T\,(\mathbf{D}\,\mathbf{D}^T)^{-1}$, to solve (27) for $\boldsymbol{\tau}$. There are two primary reasons to use the minimum two-norm solution. For an underspecified $m \times n$ matrix where $m \leq n$, this is the most well-known

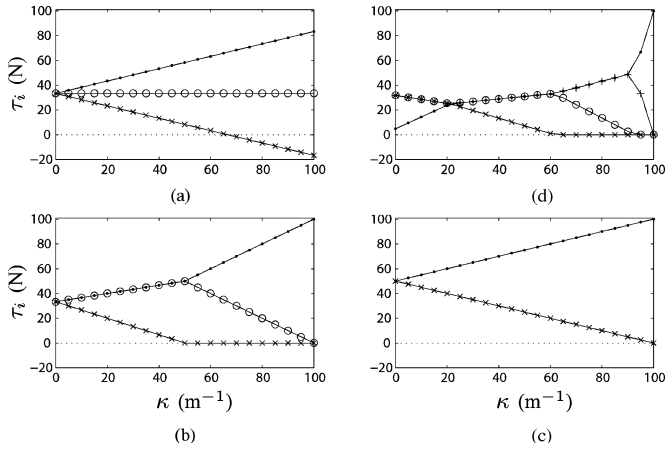

Fig. 12. Simulated tensions for planar articulation. Axial compression held constant at 10% for all simulations. (a) Minimum-norm solution for three tendons located at 1 mm (dots), 0 mm (circles), and -1 mm (x's) from centroid. (b) Minimax solution for three tendons. (c) Unique solution for two tendons. (d) Minimax solution for four tendons with fourth tendon located at 0.85 mm (crosses) from the centroid.

inversion method and it has a tractable, closed-form solution. The second reason is that, generally speaking, we prefer to have low tendon forces. This approach minimizes the two-norm of the tendon forces and is a reasonable starting point. The motivation for minimizing tendon force is because it drives a host of design requirements (i.e., motor selection, tendon yield strength, etc.).

Fig. 12(a) plots the results of the minimum-norm simulation. When the manipulator is straight ($\kappa = 0$), all three tendons are in equal tension. As the curvature is increased, the flexor tendon increases in tension while the extensor lets off in tension. A zero crossing occurs at $\kappa \approx 67$, and thereafter, the minimum-norm solution commands a negative tension. This is because a negative sign is inconsequential in a norm that squares values and because the minimum-norm method does not explicitly enforce the constraint $\boldsymbol{\tau} \geq \mathbf{0}$. This illustrates that the input filter (35) may be a necessary condition for a positive tendon tension but is not sufficient.

Looking closely at Fig. 12(a), we notice that at the maximum curvature, only one tendon has negative forces. Since $\mathbf{D} \in \mathbb{R}^{2\times 3}$ is full rank, and $n - m = 1$, we have 1 DOF in choosing $\boldsymbol{\tau}$. Therefore, we can imagine taking this single tendon and increasing its tension while the others adjust accordingly. In other words, it is possible to find some other solution that has nonnegative tendon tensions (we know this solution exists from our initial choice of $\mathbf{q}_{\mathrm{des}}$).

C. Minimax Solution

In the minimum-norm simulation of Fig. 12(a), we would have liked to have enforced the inequality constraint $\boldsymbol{\tau} \geq \mathbf{0}$, thereby avoiding slack tendons at high curvature. Furthermore, even before the zero crossing, the tendon force distribution could be improved. Therefore, the two-norm might not be the most appropriate choice of optimization criteria for this particular application. These two issues motivate us to explore alternative optimization schemes for resolving redundancy in $\mathbf{D}$ while maintaining required constraints.

As we previously mentioned, lower tendon forces are preferable. For redundantly actuated parallel manipulators, Fang *et al.* [13] minimized the sum of tendon forces and Muller [14] minimized a weighted sum of squares. For our application, perhaps a more appropriate goal than minimizing a combination of tendon forces is to prevent any single tendon from experiencing excessive force. This is justifiable since both performance and design requirements are limited by the worst case of any single tendon. Therefore, we state an alternate control objective of minimizing the maximum tendon force (infinity-norm) using only positive tensions

$$\begin{aligned} \text{minimize} \quad & \max_i(\tau_i) \\ \text{subject to} \quad & \mathbf{K}^{-1}\,\mathbf{D}\,\boldsymbol{\tau} = \mathbf{q} \\ & \boldsymbol{\tau} \geq \mathbf{0}. \end{aligned} \tag{37}$$

In this optimization problem, the constraints are linear equalities or inequalities and the objective function is piecewise linear convex. Therefore, we can apply techniques from linear programming (LP) to solve for the optimal tendon forces. Conventional LP solver routines require the problem be posed in the general form [27]. Therefore, we recast (37) with an equivalent problem using an augmented decision variable $\tilde{\mathbf{x}}$

$$\begin{aligned} \text{minimize} \quad & \tilde{\mathbf{c}}^T\,\tilde{\mathbf{x}} \\ \text{subject to} \quad & \tilde{\mathbf{A}}_{\mathrm{eq}}\,\tilde{\mathbf{x}} = \tilde{\mathbf{b}}_{\mathrm{eq}} \\ & \tilde{\mathbf{A}}\,\tilde{\mathbf{x}} \leq \tilde{\mathbf{b}} \end{aligned} \tag{38}$$

where the augmented vectors and matrices are

$$\begin{aligned} &\tilde{\mathbf{x}} = \begin{bmatrix} \boldsymbol{\tau} \\ z \end{bmatrix}, \qquad \tilde{\mathbf{c}} = \begin{bmatrix} \mathbf{0} \\ 1 \end{bmatrix} \\ &\tilde{\mathbf{A}} \begin{bmatrix} \mathbf{I} & -\mathbf{1} \\ -\mathbf{I} & \mathbf{0} \end{bmatrix}, \qquad \tilde{\mathbf{b}} = \mathbf{0} \\ &\tilde{\mathbf{A}}_{\mathrm{eq}} = [\mathbf{K}^{-1}\,\mathbf{D}, \mathbf{0}], \qquad \tilde{\mathbf{b}}_{\mathrm{eq}} = \mathbf{q}. \end{aligned} \tag{39}$$

Note that from the top row of the inequality in (38), z is an upper bound on any τ_i. Therefore, the smallest possible value of z is the maximum τ_i. Given that $\mathbf{q}$ has passed through the filter (35), a feasible solution to the LP problem (38) can now be computed.

Analogous to the minimum-norm simulation, we use the model of Fig. 11 with the same $\mathbf{q}_{des}$ to generate the minimax solution $\boldsymbol{\tau}$ plotted in Fig. 12(b). The first notable result is that there are no negative tendon forces. Having eliminated these fictitious forces found in the minimum-norm solution, we may now realistically accomplish the articulation goal.

The second key benefit of the minimax solution is found in the load distribution at smaller articulations seen in Fig. 12(a) and (b). When all tendons are in tension, the maximum force at a given curvature is indeed smaller for the minimax than in the minimum-norm simulation.

We can best understand the minimax solution by considering how one might choose to redistribute tendon loads if starting

from the minimum-norm solution in this basic three-tendon case. As an example, take the values of $\boldsymbol{\tau}$ in Fig. 12(a) at $\kappa = 40$. Since we have 1 DOF, we could start to relieve the flexor tendon that has the highest tension. To compensate for the resulting loss in curvature, we would need to decrease the load on the antagonistic extensor tendon. The compression could only be maintained by then increasing the tension on the centroidal tendon. Repeating this procedure, the centroidal tendon would eventually reach the force level of the flexor tendon force and any further adjustment would raise it above, thereby increasing the maximum. This is exactly the minimax solution in Fig. 12(b).

From this last example, the benefit of redundant tendons becomes apparent. Without a third tendon providing redundancy, there is only one unique solution, and therefore, no mobility. This case is demonstrated in Fig. 12(c) simulating a manipulator with only the two outer tendons. The maximum tendon force for a given articulation is higher than if a redundant centroidal tendon is used for optimally distributing the loads.

The three-symmetric-tendon model is useful for conceptualizing results. However, the minimax solution is also capable of solving more complex models for which the solutions are less obvious. In Fig. 12(d), we simulate a manipulator with a fourth tendon. This additional tendon further minimizes the maximum force, but in a manner that is more difficult to rationalize.

It seems from the results in Fig. 12 that the minimax solution is preferable to the minimum two-norm. However, there is one key difference that makes minimax less attractive and that is the computational burden. Although numerical methods for linear programming can guarantee bounded convergence, the exact number of iterations is not known. This can pose a problem for real-time systems with tight computational resource constraints. There are alternatives to running an online LP solver. One might store a complete solution map in memory or even design a closed-form mathematical model that emulates the minimax results. Nevertheless, computation remains a challenge for the minimax solution.

D. Real-Time Experimental Data

To validate the combination of input filter (35) and model (30) with redundancy resolution, we implement a real-time controller based on the topology in Fig. 9. The catheter used for these experiments is the same four-tendon spatial manipulator that we project onto a bend plane[1] that cuts through two antagonistic tendons. We compute the minimax solution in this plane by fully specifying the system with an appropriate additional constraint to mimic the behavior in Fig. 12(b). The resulting $\mathbf{D}$ matrix is then square and full rank making it easily invertible in real time.

We assess performance by the ability to track the desired curvature and compression in a single plane. The model parameters used were taken from the single-tendon experiments of Fig. 6. Our results are plotted in Fig. 13 and show fairly accurate tracking over a range of articulations. The curvature again is measured by locating a specific point, and therefore, is an estimate of the entire shape. All articulations were approached

[1]Planar projections are suitable given the constraint of zero out of plane moment. Therefore, the 3-D case is a straightforward extension in [28].

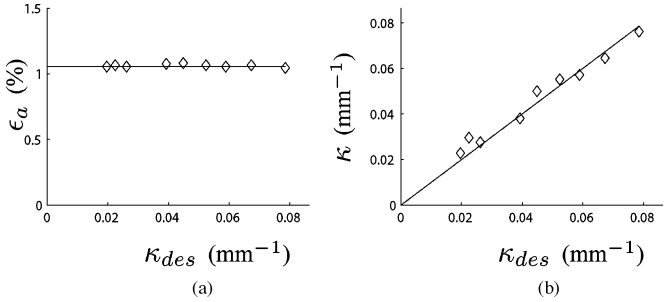

Fig. 13. Real-time control results for minimax solution of (30). Compares commanded (solid line) and measured (diamonds) values. (a) Axial compression. (b) Curvature.

in flexion and yet tracking performance does not appear to have significant bias associated with hysteresis. This could be due to the antagonistic tendon actuation and preload whereas in the mechanics experiments, we articulated only a single tendon.

These results demonstrate a successful implementation of our model accounting for the physical constraints of tendon actuation.

V. Conclusion and Future Work

The principle result from the theory and experiments presented earlier is the forward and inverse kinematic mapping between n tendon displacements and beam configuration. Of significant importance is the understanding of which input commands are feasible with a positive tendon tension, and how they might be achieved with redundant tendons. The mechanics-based model can be used to minimize occurrences of slack tendons, optimize pull wire force distribution, provide robust tracking, and calculate manipulator configuration from multiple tendon displacements.

The main purpose of this study was to elucidate the underlying mechanics of tendon-driven continuum manipulators. For the sake of clarity, we studied the simplest case of a planar, single-section manipulator. It is our intention for this simple case to serve as a module in higher complexity models and control systems.

Our method of measuring the manipulator configuration by eyesight is a laborious process and only suitable to planar measurements. Therefore, our ongoing research is aimed at developing a vision-based sensor for estimating the manipulator configuration automatically in 3-D. The development of a 3-D sensor system will be accompanied by the extension of our planar model to 3-D in [28].

Another use of this model is for task-space control [29]. This could be accomplished with an additional transformation from the distal tip Cartesian coordinates to beam configuration such as the D–H approach suggested in [18]. When working in task-space, cascading manipulator sections serially becomes attractive for increasing end-effector mobility. Our model could be extended to include mechanical couplings among sections with the possibility of decoupling their motion. Lastly, we can imagine various sensor inputs and control loops combined with this mechanics model for dealing with internal model errors and otherwise unknown external disturbances.

REFERENCES

[1] P. Dario, B. Hannaford, and A. Menciassi, "Smart surgical tools and augmenting devices," *IEEE Trans. Robot. Autom.*, vol. 19, no. 5, pp. 782–792, Oct. 2003.

[2] R. Taylor, "Robots as surgical assistants: Where we are, wither we are tending, and how to get there," in *Proc. AIME*, 1997, pp. 3–11.

[3] G. Ballantyne and F. Moll, "The da vinci telerobotic surgical system: The virtual operative field and telepresence surgery," *Surg. Clin. North Amer.*, vol. 83, no. 6, pp. 1293–1304, 2003.

[4] R. Satava, "Emerging technologies for surgery in the 21st century," *Archives Surg.*, vol. 134, no. 11, pp. 1197–1202, 1999.

[5] D. Camarillo, T. Krummel, and J. Salisbury, "Robotic technology in surgery: Past, present, and future," *Amer. J. Surg.*, vol. 188, no. 4A, pp. 2S–15S, 2004.

[6] G. Robinson and J. Davies, "Continuum robots—A state of the art," in *Proc. IEEE ICRA*, vol. 4, Detroit, MI, 1999, pp. 2849–2854.

[7] J. Bacher, C. Joseph, and R. Clavel, "Flexures for high precision robotics," *Ind. Robot.*, vol. 29, no. 4, pp. 349–53, 2002.

[8] J. Simo and L. Vu-Quoc, "On the dynamics of flexible beams under large overall motions—The plane case part 1," *J. Appl. Mech.*, vol. 53, no. 4, pp. 849–863, 1986.

[9] I. Gravagne, C. Rahn, and I. Walker, "Large deflection dynamics and control for planar continuum robots," *IEEE/ASME Trans. Mechatronics*, vol. 8, no. 2, pp. 299–307, Jun. 2003.

[10] S. Hirose, *Biologically Inspired Robots, Snake-Like Locomotors and Manipulators*, 1st ed. Oxford, U.K.: Oxford Univ. Press, 1993.

[11] S. Jacobsen, H. Ko, E. Iversen, and C. Davis, "Antagonistic control of a tendon driven manipulator," in *Proc. IEEE ICRA*, Scottsdale, AZ, 1989, pp. 1334–1339.

[12] J. K. Salisbury and J. J. Craig, "Articulated hands—Force control and kinematic issues," *Int. J. Robot. Res.*, vol. 1, no. 1, pp. 4–17, 1982.

[13] S. Fang, D. Franitza, M. Torlo, F. Bekes, and M. Hiller, "Motion control of a tendon-based parallel manipulator using optimal tension distribution," *IEEE/ASME Trans. Mechatronics*, vol. 9, no. 3, pp. 561–568, Sep. 2004.

[14] A. Muller, "Internal preload control of redundantly actuated parallel manipultors—Its application to backlash avoiding control," *IEEE Trans. Robot.*, vol. 21, no. 4, pp. 668–677, Aug. 2005.

[15] R. Verhoeven and M. Hiller, "Tension distribution in tendon-based stewart platforms," in *Proc. ARK Int. Symp. Adv. Robot Kinematics*, 2002, pp. 117–124.

[16] G. Yang, C. Pham, and S. Yeo, "Workspace performance optimization of fully restrained cable-driven parallel manipulators," in *Proc. IEEE/RSJ Int. Conf. Intell. Robots Syst.*, Beijing, China, 2006, pp. 85–90.

[17] C. Li and C. Rahn, "Design of continuous backbone, cable-driven robots," *J. Mech. Des.*, vol. 124, no. 2, pp. 265–271, 2002.

[18] B. Jones and I. Walker, "Kinematics for multisection continuum robots," *IEEE Trans. Robot.*, vol. 22, no. 1, pp. 43–55, Feb. 2006.

[19] K. Xu and N. Simaan, "Actuation compensation for flexible surgical snake-like robots with redundant remote actuation," in *Proc. IEEE ICRA*, 2006, pp. 4148–4154.

[20] A. Kapoor, K. Xu, W. Wei, N. Simaan, and R. Taylor, "Telemanipulation of snake-like robots for minimally invasive surgery of the upper airway," in *Proc. MICCAI Med. Robot. Workshop*, 2006, pp. 17–25.

[21] I. Gravagne and I. Walker, "On the kinematics of remotely-actuated continuum robots," in *Proc. IEEE ICRA*, San Francisco, CA, 2000, pp. 2544–2550.

[22] M. Higashimori, M. Kaneko, A. Namiki, and M. Ishikawa, "Design of the 100g capturing robot based on dynamic preshaping," *Int. J. Robot. Res.*, vol. 24, no. 9, pp. 743–753, 2005.

[23] S. Stein and A. Barcellos, *Calculus and Analytic Geometry*, 5th ed. New York: McGraw-Hill, 1992.

[24] J. Stoker, *Differential Geometry*. New York: Wiley, 1969.

[25] L. Kollar and G. Springer, *Mechanics of Composite Structures*. Cambridge, U.K.: Cambridge Univ. Press, 2003.

[26] F. Beer and E. Johnston, *Mechanics of materials*, 3rd ed. New York: McGraw-Hill, 2002.

[27] D. Bertsimas and J. Tsitsiklis, *Introduction to Linear Optimization*. Belmont, MA: Athena Scientific, 1997.

[28] D. Camarillo, K. Loewke, C. Carlson, and J. Salisbury, "Vision based 3-D shape sensing of flexible manipulators," *Proc. IEEE ICRA*, Pasadena, CA, 2008, pp. 2940–2947.

[29] O. Khatib, "A unified approach for motion and force control of robot manipulators - the operational space formulation," *IEEE J. Robot. Autom.*, vol. 3, no. 1, pp. 43–53, Feb. 1987.

David B. Camarillo (M'08) received the B.S.E. degree in mechanical and aerospace engineering from Princeton University, Princeton, NJ, and the M.S. and Ph.D. degrees in mechanical engineering from Stanford University, Stanford, CA.

From 2003 to 2004, he was with Intuitive Surgical, Inc., where he worked on an NIH-funded robotic endoscope project. Since 2005, he has been a Senior Controls Engineer at Hansen Medical, Inc., Mountain View, CA, developing a flexible robotic surgery system. His current research interests include modeling and control of mechatronic systems, particularly for biomedical applications.

Christopher F. Milne received the B.S.E. degree in mechanical engineering from Princeton University, Princeton, NJ, in 2001, and the M.S. degree in mechanical engineering from Stanford University, Stanford, CA, in 2005.

From 2002 to 2003, he was a Primary Mechanical Engineer at Iguana Robotics, Inc., Urbana-Champaign, IL. He is currently a Senior Systems Engineer at Hansen Medical, Inc., Mountain View, CA.

Christopher R. Carlson received the Ph.D. degree in mechanical engineering from the Dynamic Design Laboratory, Stanford University, Stanford, CA, in 2003.

He is currently a Controls Engineering Fellow at Hansen Medical, Inc., Mountain View, CA. His current research interests include modeling, identification, and control of dynamic systems with classical as well as computational tools. His favorite experimental platforms are land vehicles and medical robots.

Michael R. Zinn (M'07) received the B.S. and M.S. degrees in civil engineering from Massachusetts Institute of Technology (MIT), Cambridge, and the Ph.D. degree in mechanical engineering from Stanford University, Stanford, CA.

He was the Director of Systems and Controls Engineering at Hansen Medical, Inc. In 2007, he joined the University of Wisconsin (UW), Madison. His current research interests include understanding the design and control challenges of human-centered robotics and developing effective strategies to overcome these challenges. He is also involved in improving the performance, safety, and efficacy of robotic catheters for minimally invasive surgery through the use of advanced control, sensing, and visualization methods. He has over 10 years of electromechanical system design and control experience.

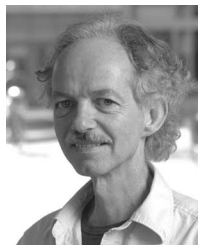

J. Kenneth Salisbury (M'80) was a Scientific Advisor for Robotics and Human Augmentation at the National Science Foundation's Advisory Council, Intuitive Surgical, Inc., and a Technical Advisor at Robotic Ventures, Inc. He is currently a Professor of computer science, surgery, and mechanical engineering at Stanford University, Stanford, CA. His current research interests include the area of robots, human–robot interactions, and computer haptics. He is also involved in fundamental issues in medical simulation and the creation of miniature surgical instruments. He is a holder of over 25 patents.